

A hybrid coupled cluster–machine learning algorithm: Development of various regression models and benchmark applications

Cite as: *J. Chem. Phys.* **156**, 014109 (2022); <https://doi.org/10.1063/5.0072250>

Submitted: 21 September 2021 • Accepted: 12 December 2021 • Accepted Manuscript Online: 13 December 2021 • Published Online: 03 January 2022

 Valay Agarawal,  Samrendra Roy,  Kapil K. Shrawankar, et al.



View Online



Export Citation



CrossMark

ARTICLES YOU MAY BE INTERESTED IN

[Accelerating coupled cluster calculations with nonlinear dynamics and supervised machine learning](#)

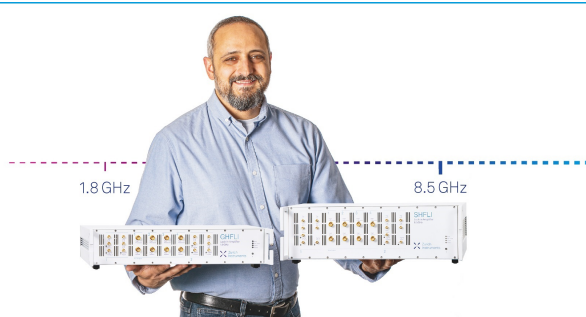
The Journal of Chemical Physics **154**, 044110 (2021); <https://doi.org/10.1063/5.0037090>

[Perturbation-adapted perturbation theory](#)

The Journal of Chemical Physics **156**, 011101 (2022); <https://doi.org/10.1063/5.0079853>

[A similarity transformed second-order approximate coupled cluster method for the excited states: Theory, implementation, and benchmark](#)

The Journal of Chemical Physics **156**, 014110 (2022); <https://doi.org/10.1063/5.0064889>



Trailblazers. 

Meet the Lock-in Amplifiers that measure microwaves.

 Zurich Instruments [Find out more](#)

A hybrid coupled cluster-machine learning algorithm: Development of various regression models and benchmark applications

Cite as: J. Chem. Phys. 156, 014109 (2022); doi: 10.1063/5.0072250

Submitted: 21 September 2021 • Accepted: 12 December 2021 •

Published Online: 3 January 2022



Valay Agarwal,¹ Samrendra Roy,² Kapil K. Shrawankar,¹ Mayank Chogale,³ S. Bharathi,¹ Anchal Yadav,¹ and Rahul Maitra^{1,a)}

AFFILIATIONS

¹ Department of Chemistry, Indian Institute of Technology Bombay, Powai, Mumbai 400076, India

² Department of Energy Science and Engineering, Indian Institute of Technology Bombay, Powai, Mumbai 400076, India

³ Institute of Chemical Technology, Mumbai 400019, India

^{a)}Author to whom correspondence should be addressed: rmaitra@chem.iitb.ac.in

ABSTRACT

The iterative solution of the coupled cluster equations exhibits a synergistic relationship among the various cluster amplitudes. The iteration scheme is analyzed as a multivariate discrete time propagation of nonlinearly coupled equations, which is dictated by only a few principal cluster amplitudes. These principal amplitudes usually correspond to only a few valence excitations, whereas all other cluster amplitudes are enslaved and behave as auxiliary variables [Agarwal *et al.*, J. Chem. Phys. **154**, 044110 (2021)]. We develop a coupled cluster–machine learning hybrid scheme where various supervised machine learning strategies are introduced to establish the interdependence between the principal and auxiliary amplitudes on-the-fly. While the coupled cluster equations are solved only to determine the principal amplitudes, the auxiliary amplitudes, on the other hand, are determined via regression as unique functionals of the principal amplitudes. This leads to significant reduction in the number of independent degrees of freedom during the iterative optimization, which saves significant computation time. A few different regression techniques have been developed, which have their own advantages and disadvantages. The scheme has been applied to several molecules in their equilibrium and stretched geometries, and our scheme, with all the regression models, shows a significant reduction in computation time over the canonical coupled cluster calculations without unduly sacrificing the accuracy.

Published under an exclusive license by AIP Publishing. <https://doi.org/10.1063/5.0072250>

I. INTRODUCTION

Coupled cluster (CC) theory^{1–4} is a well established method for solving the electronic Schrödinger wave equation for small to medium sized atoms and molecules. CC theory employs an exponential wave operator Ω that brings in the effects of the excited Slater determinants on to the reference ground state wavefunction, which is usually taken to be the Hartree–Fock determinant. The wave operator Ω is chosen as $\Omega = e^T$, where T is the sum of all possible many-body hole to particle excitation operators. In the most common cases, T consists of one- and two-body hole–particle excitation operators. The resultant theory, known as the CC with singles and doubles excitations (CCSD), predicts quite accurate energies for molecules with predominantly single reference character. The amplitudes corresponding to the excitation operators, which are

the unknown quantities, are determined by projecting the similarity transformed effective Hamiltonian $G = e^{-T}He^T$ against the excited state determinants. The correlated ground state energy is calculated as the expectation value of the effective Hamiltonian with respect to the chosen reference function, $E_{corr} = \langle \phi_{HF} | H_{eff} | \phi_{HF} \rangle = \langle \phi_{HF} | e^{-T}He^T | \phi_{HF} \rangle$. Due to the exponential nature of the wave operator, the similarity transformed Hamiltonian, H_{eff} , is highly nonlinear in T , and hence, one employs an iterative scheme to solve these equations. For CCSD, the most expensive computational step scales as $n_o^2 n_v^4$ per iteration, where n_o is the number of the occupied orbitals and n_v is the number of the virtual orbitals in the chosen reference determinant. This often makes the theory prohibitively time consuming for large systems. The theory since its inception has seen many developments to increase its accuracy with a reduced computational scaling. Due to the iterative nature of the solutions,

there have been significant efforts to accelerate the convergence^{5–8} or scale down the steep computational scaling associated with the solution scheme.^{9–12} One may thus look for an iterative scheme where the expensive $n_o^2 n_v^4$ scaling may be bypassed, at least partially, which is likely to save a lot of computation time. This may be achieved by exploiting the nonlinearity of the iterative solution scheme. In line with this, some of the present authors imbibed ideas from nonlinear dynamics and synergetics^{13–15} to demonstrate that not all the cluster amplitudes are equally important in the nonlinear iteration scheme. Based on the magnitude of the amplitudes, the authors classified the amplitudes into “unstable master amplitudes” (later to be referred to as the principal amplitudes) and “stable slave amplitudes” (later to be referred to as the auxiliary amplitudes). Borrowing the key concepts from nonlinear discrete time-series,^{16,17} coupled with principles imported from the areas of synergetics, a Machine Learning (ML)¹⁸ based hybrid numerical scheme was developed to establish a relationship between the two classes of amplitudes. This effectively reduces the independent degrees of freedom to accelerate the overall iteration process. In the resulting scheme, only a few initial iterations scale as $n_o^2 n_v^4$, while most of the other iterations scale significantly less. This saves a lot of computation time, as was demonstrated by the authors. Complementary to that, one may employ an adiabatic approximation based on the difference in the time scale of relaxation of various cluster amplitudes during the iteration, where one may formally reduce the scaling of the iterative scheme by at least one order of magnitude, without undue sacrifice of the accuracy.

In this context, it may superficially appear that our development follows the same line of thought as methods such as coupled-cluster single double triple coupled cluster with singles doubles and triples excitations (CCSDT)-n^{19,20} or various renormalized CC^{21,22} theories where one determines the important amplitudes iteratively while less important ones are treated in a non-iterative manner. Unlike the methods mentioned above, our approach relies upon choosing the important amplitudes based on macroscopic convergence pattern, rather than any many-body perspective. In most cases, the amplitudes that are important from a many-body consideration (such as those corresponding to the valence excitations) are the same as those that dictate the macroscopic convergence; however, this is not always strictly the case. In addition, in recent years, there has been increasing attention to adaptive solutions to differential equations, which broadly follow the same line of thought as the present work. One such approach in electronic structure calculations was put forward by Beylkin *et al.* where the authors had chosen the “best” subset of linearly independent terms from a large pool of Gaussian mixtures to solve iterative nonlinear equations. This approach²³ has been quite successful in solving Hartree–Fock equations with reduced computational scaling. Such adaptive methods have strong connections to neural nets and machine learning as well.

In Sec. II, we discuss the essential aspects of the newly developed iteration scheme, where we reiterate the existence of a circularly causal relationship among the principal and the auxiliary amplitudes. We will show how a machine learning strategy can be employed based on the circular causality to simplify coupled cluster calculations. In Sec. III, we discuss each of the machine learning models and their performance in terms of accuracy and time requirements. We will discuss four models out of which three

are primarily regression based and the last one is a classification based model. In Sec. IV, we conclude our findings with overarching remarks on the performance of the models.

II. NONLINEARITY IN THE CC ITERATION SCHEME FROM SYNERGISTIC PERSPECTIVE AND OVERVIEW OF A NEW ALGORITHM BASED ON THE CIRCULAR CAUSALITY RELATIONSHIP

The slaving principle states that there exists a nontrivial relationship among the set of most significant and less significant cluster amplitudes during the nonlinear iteration process. While the significant amplitudes dictate the iteration process in the macroscopic sense, other less significant amplitudes are simply *enslaved*, and their variation gets suppressed. These significant amplitudes, which are large in magnitude and mostly labeled by the active orbitals, are interchangeably termed the principal or the driver amplitudes. From the viewpoint of the nonlinear discrete time dynamics, they are the unstable modes and are denoted by t^L . The space spanned by them is termed the large amplitude subset (LAS), having dimension n_L . On the other hand, the amplitudes with lesser magnitudes than a pre-defined threshold have significantly less importance in the iteration dynamics, and they are the stable modes of the time-discrete iteration process. They are termed the auxiliary amplitudes, denoted by t_S , which span the small amplitude subset (SAS) with dimension n_S . Note that $n_S \gg n_L$. The principal and the auxiliary amplitudes are known as master and slave variables, respectively, in synergetics. Technically, when the system of amplitude equations are sufficiently perturbed from the fixed point equilibrium, one may get a set of unstable modes from the eigenvalues of its stability matrix. Thus, the amplitudes (or combinations thereof) corresponding to the modes with positive Lyapunov exponents are the ones which are to be interpreted as the principal amplitudes of the iteration dynamics that approximates an effective Hamiltonian flow. In one of our earlier publications,²⁴ the authors had analyzed a detailed structure of the stability matrix and its connection to the equation of motion, and hence, it is not discussed any further here. One must note that within the fixed point equilibrium region, there is no simple mathematical protocol to extract out the unstable modes, and in the present work, some of the primitive amplitudes with magnitude greater than a cutoff are taken as the principal ones. While the two-body amplitudes are chosen based on their relative magnitudes at the MP2 level by setting a pre-defined cutoff value ($\epsilon = [0.014–0.018]$), the classification of the one electron excitation amplitudes is performed at the lowest order, i.e., $T_1 \leftarrow (VT_2^{MP2})_c$, where $(\dots)_c$ stands for the connected terms and the same cutoff is used as T_2 .

Following our earlier work, we conjecture that even in the fixed point equilibrium, when the system is not sufficiently perturbed, there still exists a mapping F , at least numerically, such that

$$F : t_k^L \rightarrow t_k^S \quad (1)$$

where k is the discrete time iteration step. We established that one may numerically exploit this mapping to reduce the computational time required for the coupled cluster calculations. Please note that in our scheme, the excitation amplitudes are all entangled. They are separated insofar as the difference of CC diagrams is concerned, but while defining the LAS and SAS, neither the two-body amplitudes

are treated in a separate footing from the one-body amplitudes nor vice versa. In our scheme, both the sets of one-body and two-body amplitudes are treated in the same footing.

In order to establish the mapping F as shown in Eq. (1), one may modify the CC iteration scheme based on the circular causality that exists between the principal and the auxiliary amplitudes. This is shown in Fig. 1. However, the circular causality presumes that the map F is known. In order to establish the mapping, one may use the routine CC framework to calculate both the sets of amplitudes: t^L and t^S . After a certain number of *training* iterations, the principal amplitudes are extracted, and they are trained to map on to the auxiliary amplitudes for once. This mapping in our current scheme is done via various kernelized regression based ML models where the principal amplitudes are taken as the independent input variables and the auxiliary amplitudes are the dependent variables that are predicted. For each individual molecular/atomic calculation, this training needs to be done right after the initial iterations only once, and there is no requirement of any previously computed data. Our model can be trained on the amplitudes on the fly during the iteration process. Depending on the desired level of accuracy, we will present four different regression models that have their own advantages and disadvantages, and we will discuss those in the sections to follow along with their exhaustive numerical applications. Once the amplitudes are trained and the functional form of F which maps t^L on to t^S is numerically established, the algorithm runs via the circular causality loops as shown in Fig. 1. This consists of two steps: in step-I, all the auxiliary amplitudes are determined from the principal amplitudes of the same iteration time step via the ML regression model. In step-II, the principal amplitudes are updated via the feedback coupling of both sets of the amplitudes. This circular causality loop continues until the principal amplitudes (and, hence, the auxiliary amplitudes, due to the fixed functional dependence) converge. Note that in step-II, only the principal amplitudes are determined

through the exact CC equations, although the auxiliary amplitudes that are plugged in are obtained via ML. The computational scaling of this step is $n_L n_v^2 n_v 2$ as demonstrated by Agarawal *et al.*²⁵ Since n_L is only a very small fraction even compared to $n_o n_v$, this step has a significant reduction in scaling from the usual $n_o^2 n_v^4$ of the conventional scheme. Step-I involves only a single matrix multiplication, and hence, it scales negligibly compared to step-II. We will henceforth refer to this algorithm as the hybrid CC-ML scheme.

The computational time requirement by the overall hybrid CC-ML scheme is governed by two major factors: (1) the number of conventional iterations (m) used to train the model to determine F and (2) the dimension of the LAS, n_L . Simple calculations show that over 90% of the overall calculation time is consumed in generation of data through the initial iterations and training of model. Thus, there is a lot of scope to play around with different ML models that can predict the auxiliary amplitudes with fewer training iterations and minimize the required dimension of the LAS, n_L , without unduly sacrificing the accuracy.

In a previous publication, Agarawal *et al.*²⁵ had studied the efficacy of the Kernel Ridge Regression (KRR) based ML model to represent F . This was studied for a few pilot molecules in their equilibrium and away from equilibrium geometries, and it produced highly accurate energies [of the order of micro-Hartree (μH), compared to the canonical CC calculations]. The authors also systematically studied the time requirements necessary for the overall process, and as expected, it was much less than the conventional CCSD scheme. In fact, in order to obtain a sub- μH accuracy in energy, the time requirement for the algorithm was similar (or lower) to that of a DIIS accelerated CC scheme. Thus, the pilot study showed extremely promising results, and it required further benchmarking. In this paper, we have thoroughly studied the performance of the KRR model, both in terms of energy accuracy and time requirement, for about 60 molecular applications with various degrees of electronic complexity. We would also introduce a few more regression models, which would further greatly reduce the requirements of the numbers of initial training iterations, and the LAS dimension. All the models will be thoroughly benchmarked with numerous numerical applications.

III. DISCUSSION ON VARIOUS REGRESSION BASED MACHINE LEARNING MODELS AND THEIR BENCHMARKING STUDIES

In this section, we will describe various regression based ML models that have been employed in this work. We have studied four different regression models to represent the forward mapping (step-I) of the circular causality loop. The models which we would be considering in this paper are as follows:

- Kernel Ridge Regression (KRR),
- Customized Kernel Regression (CKR),
- Polynomial-Kernel Ridge Regression (PKR), and
- K-Nearest Neighbors (KNN).

Following the initial iteration cycles, the model is trained only once for each molecule after which the iteration runs through the circular causality loop. In all the ML models, the input parameters are the principal amplitudes, t^L , which are taken to be the independent variables, and the output is the set of auxiliary amplitudes

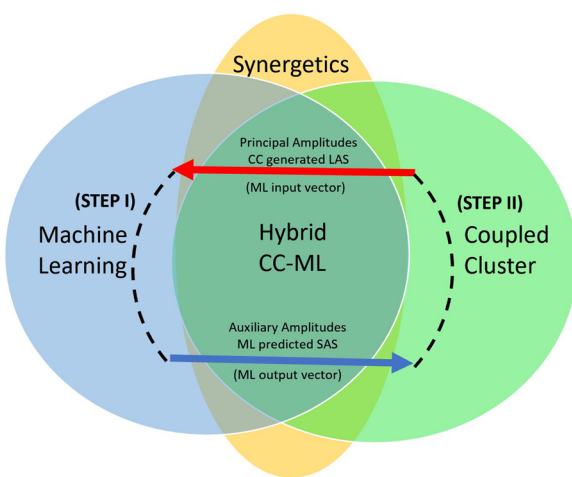


FIG. 1. General structure of the circular causality loop: the principal amplitudes are mapped on to the auxiliary amplitudes using a ML model (step-I) and their feedback coupling to obtain the updated set of the driver amplitudes via step-II. This loop is constructed following the initial iteration cycles and training of the relevant ML model.

t^S which are predicted. While CKR and PKR models superficially have the similar working philosophy to that of KRR, they differ from KRR in the detailed structure of the kernel matrix. Hence, the underlying mathematical structure of all these three models will be discussed together in the section that deals with KRR. In the subsequent sections dealing with CKR and PKR models, we will only present the kernelization techniques which distinguish them from KRR. We should also mention that ML techniques such as neural networks or random forest appear to be much less accurate and data intensive. In our pilot implementation with these methods, it was found that they necessitate too many training iterations for giving substantially accurate results; otherwise, it produces somewhat poor accuracy with comparable data requirements. Furthermore, another caveat with using neural networks would be that the calculations necessarily need to be performed on a Graphics Processing Unit (GPU) to give any decent time requirement, which makes the comparison tricky as the CC calculations are done on a central processing unit (CPU), and hence, they were not considered any further for this paper. In the following, we will briefly present the working principles of all the different models that we considered and would also present the benchmarking applications along with the comparison to the canonical CCSD results. For each molecule, both the canonical CCSD and hybrid CC–ML calculations were done in the same machine for proper comparison of the relative computation timing. In addition, both CC–ML (for generation of the training dataset) and CCSD scheme used the same program with same level of optimization.

A. Development of the kernel ridge regression model

1. Formal aspects and structure of the working equations

In this subsection, we will discuss the main ideas behind the kernel ridge regression model. As mentioned before, this model also forms the base for two other models under consideration, namely, the customized kernel regression and the polynomial kernel ridge regression. The KRR model is strictly based on the linear regression algorithm. A linear regressor fits the dependent auxiliary amplitudes as a linear function of the independent principal amplitudes. The training of model essentially translates to finding appropriate coefficients in a linear function of principal amplitudes to give auxiliary amplitudes. As one would expect, the accuracy of the function would be directly dependent on the number of training iterations m .

As mentioned previously, during the training cycles, the CC equations are iterated in the full space spanned by $\{t^L \oplus t^S\}$ amplitudes, and these exact amplitudes are used to train the model. During the training, the entire space of $\{t^L \oplus t^S\}$ is processed into two matrices of T^S and T^L , where T^L is defined as

$$T^L = \begin{pmatrix} 1 & t_{11}^L & t_{21}^L & \dots & t_{n_L 1}^L \\ 1 & t_{12}^L & t_{22}^L & \dots & t_{n_L 2}^L \\ 1 & t_{13}^L & t_{23}^L & \dots & t_{n_L 3}^L \\ \vdots & \vdots & \vdots & \ddots & \vdots \\ 1 & t_{1m}^L & t_{2m}^L & \dots & t_{n_L m}^L \end{pmatrix}. \quad (2)$$

Here, each row signifies the n_L independent principal cluster amplitudes for a given iteration. With m number of training iterations

performed to construct the T^L matrix, it is of the dimension $m \times (n_L + 1)$. The extra column in T^L is added to take care of the intercept term. A generalized linear fit can be written in the form of $T^S = T^L \beta$, where β is the coefficient matrix of the linear functions of t^L . It can be trivially defined as

$$\beta = \begin{pmatrix} \beta_{01} & \beta_{02} & \beta_{03} & \dots & \beta_{0n_s} \\ \beta_{11} & \beta_{12} & \beta_{13} & \dots & \beta_{1n_s} \\ \beta_{21} & \beta_{22} & \beta_{23} & \dots & \beta_{2n_s} \\ \vdots & \vdots & \vdots & \ddots & \vdots \\ \beta_{n_L 1} & \beta_{n_L 2} & \beta_{n_L 3} & \dots & \beta_{n_L n_s} \end{pmatrix}, \quad (3)$$

where n_s , as mentioned before, is the number of the elements in the dependent SAS amplitudes for a given iteration. Thus, the matrix T^S is of the dimension $m \times n_s$, defined as

$$T^S = \begin{pmatrix} t_{11}^S & t_{21}^S & \dots & t_{n_s 1}^S \\ t_{12}^S & t_{22}^S & \dots & t_{n_s 2}^S \\ t_{13}^S & t_{23}^S & \dots & t_{n_s 3}^S \\ \vdots & \vdots & \vdots & \vdots \\ t_{1m}^S & t_{2m}^S & \dots & t_{n_s m}^S \end{pmatrix}. \quad (4)$$

Starting from a guess coefficient matrix, $\hat{\beta}$, the optimized coefficients may be obtained by minimizing the loss function $\eta^T \eta$. Here, η is the error function defined by $\eta = T^S - \hat{T}^S$, where $\hat{T}^S = T^L \cdot \hat{\beta}$ is the predicted auxiliary amplitude matrix obtained during the training cycles. With m training iterations, $\hat{\beta}$ can be optimized to give β , which will be used for prediction in the subsequent iterations.

One may further increase the power of the independent principal amplitudes to quadratic and cubic to capture the nonlinear features of the trajectory. This leads to an increase in the dimension on the independent variable space, and hence, there is a better chance of getting a better fit. One thus increases the independent variable space from a dimension of n_L to a higher dimensional space by including polynomial forms of t^L and treats each term as an independent variable. Let the higher dimension space with nonlinear terms be connected to the feature vectors by a map ϕ , which can be defined as

$$\phi : \{t_\mu^L, \mu \in n_l\} \rightarrow \{t_\mu^L, t_\mu^L t_\nu^L, \dots, (t_\mu^L)^d, \mu, \nu \in n_l\}, \quad (5)$$

where d is the degree of the polynomial. The loss function now becomes $\hat{\beta}_\mu = \phi^T (\phi \phi^T)^{-1} (T_\mu^S)$. The whole operation, if done directly, is expensive, and one usually makes use of the kernelization technique instead, which allows for evaluation of the expression without explicit knowledge of the function ϕ .

According to the Mercer theorem,²⁶ one may define the kernel function $K = \phi \phi^T$ for every symmetric positive definite matrix. Thus, the loss function now becomes $\hat{\beta}_\mu = \phi^T (K)^{-1} (T_\mu^S)$. After sufficient training of the model, the auxiliary SAS amplitudes for the i th iteration ($i > m$) (t_i^S) are predicted using only the optimized coefficient matrix and the LAS amplitude vector of the same iteration (t_i^L),

$$t_{\mu,i}^S (\text{predicted}) = \phi(\{t_i^L\}) \hat{\beta}_\mu. \quad (6)$$

Note that the effect of t^S or previous iterations is included in the β matrix.

To bypass the usage of ϕ , a new kernel function K_L is defined, which takes all the previous training amplitudes and the t_i^L to predict the t_i^S . Thus, $K_L = \phi(\phi(t_i^L))^T$, where the right most ϕ appearing in the above equation is a function of t_i^L ,

$$t_{pred}^S = (K_L)^T K^{-1} T^S. \quad (7)$$

Here, the subscript indicates that these are the predicted SAS amplitudes.

To avoid unphysical underfitting or overfitting due to erroneous weight in the training dataset, a regularization parameter is introduced, which penalizes the model each time a certain term gets unphysical weight. Thus, one may modify Eq. (7) by adding a regularization term as

$$t_{pred}^S = (K_L)^T (K + \lambda I)^{-1} T^S. \quad (8)$$

Following the convention, we denote the regularization parameter with α . Here, $\lambda = \alpha/2$. The value of $\lambda(\alpha)$ manages overfitting at the cost of the rate of learning. A small value of α trains a model very quickly and often overfits the data points, which could result in slight inaccuracies with few training datasets. On the other hand, a large α slows down the learning process, and the model takes a larger number of training datasets to produce accurate results. Thus, the value of α requires tuning.

In Eq. (8), we note that the quantity $(K + \lambda I)^{-1} T^S$ can be computed only once for all after the training dataset is produced. Thus, all the t_i^S amplitudes may be computed each iteration via a single matrix multiplication of $(K_L)^T$ and $(K + \lambda I)^{-1} T^S$ instead of algebraically or diagrammatically solving the coupled cluster equations, which results in savings in the overall computational time. We must also note that all these processes are already standardized in scikit,²⁷ and one has to only supply T^L and T^S for training.

In an earlier paper, we had presented a few pilot molecular applications to show the potential of the hybrid CC-ML(KRR) method. However, a more thorough analysis of the model on a large number of molecules with varying electronic complexities is necessary to show the efficacy of the method with statistical significance. We have employed the KRR model to study the ground state energetics of 59 cases with different molecules/geometries/basis sets. In Subsection III A 2, we will study the efficacy of the KRR model in terms of accuracy in predicted energy compared to CCSD and the associated time requirements.

2. Assessment of the performance of KRR model

The accuracy of any regression method largely depends on the number of iterations used to train the model. As expected, the larger the training iterations employed, the better would be the accuracy. In the first row of Fig. 2, we have plotted the difference in the energy obtained via canonical CCSD and our hybrid CC-ML(KRR) model for 6, 7, and 8 training iterations for 60 different combinations of molecules, basis sets, and geometries. See the [supplementary material](#) for further information on the molecules, geometries, and basis sets employed in this study. With six training iterations, for most of the molecules in their respective equilibrium geometries, the hybrid CC-ML(KRR) predicts energy, which is accurate up to 2 μH to the

exact CCSD energy. However, there are quite a few cases, particularly for molecules in distorted geometries, for which six training iterations are not sufficient to accurately determine F , and they provide results which are off by a large margin. They are not included in the scale of the plot. However, with a higher number of training iterations, the difference between the energy obtained via canonical CCSD and hybrid CC-ML(KRR) tends to converge more toward the middle. This is particularly true for molecules in away from their equilibrium geometries, which are shown by the red dots. The mean absolute deviation (MAD) for molecules in away from equilibrium regions converges very fast with the number of training iterations from MAD = 16.0 μH with $m = 6$ to MAD = 6.4 μH with $m = 7$ to MAD = 2.6 μH with $m = 8$. For the molecules in their equilibrium geometries, even with six training iterations, a MAD of 1.2 μH is observed, which further systematically improves as we increase the number of training iterations. Overall, irrespective of the molecular geometry, with $m = 7$, the CC-ML(KRR) predicts energy within $\pm 2 \mu\text{H}$, which is shown by the yellow band.

In the second row of Fig. 2, we have plotted the fraction of the time taken by the hybrid CCSD-ML(KRR) scheme compared to the conventional CCSD calculations. With $m = 6$, the hybrid CC-ML(KRR) scheme takes around 61% time compared to the conventional CCSD calculations for molecules in the equilibrium geometries. For the molecules with away from equilibrium geometries, the hybrid CC-ML(KRR) on an average takes around 49% of the total computational time to that required for the CCSD. As one includes more training iterations, the time requirement increases, and the scattered points shift upward. One may also note that the blue points (which are assigned for molecules with equilibrium geometries) appear higher than the red points (for molecules with stretched geometries). This is due to the fact that the molecules in equilibrium geometries take a much lesser number of CCSD iterations to converge, and hence, the training cycles take a large fraction of the overall calculation. In stretched geometries, the CCSD calculations take longer time to converge, which means that for the hybrid CC-ML scheme, the cost of initial iterations and training of the model is small relative to the total computation time, and hence, the red dots appear consistently below the blue points. Note that with eight training iterations, the computation time ratio is only 0.72 and 0.55 for equilibrium and away from equilibrium geometries, respectively, relative to the canonical CCSD calculations. In the case where the CCSD scheme is accelerated via DIIS, the ratio is slightly higher, as expected and observed from the third row of Fig. 2. However, the hybrid CC-ML(KRR) still outperforms DIIS accelerated CCSD in terms of the required computational time for most cases irrespective of the molecular geometry.

B. Development of the customized kernel regression model

1. Formal aspects and structure of the working equations

While the hybrid CC-ML(KRR) model is very stable and accurate, it requires a larger number of training sets. Moreover, one needs to start with an unknown polynomial form of the coupling map. Moreover, in the CC-ML(KRR) model, even starting from the first order guess amplitudes, one needs to discard a couple of initial iterations as the iteration pattern does not get stabilized to be

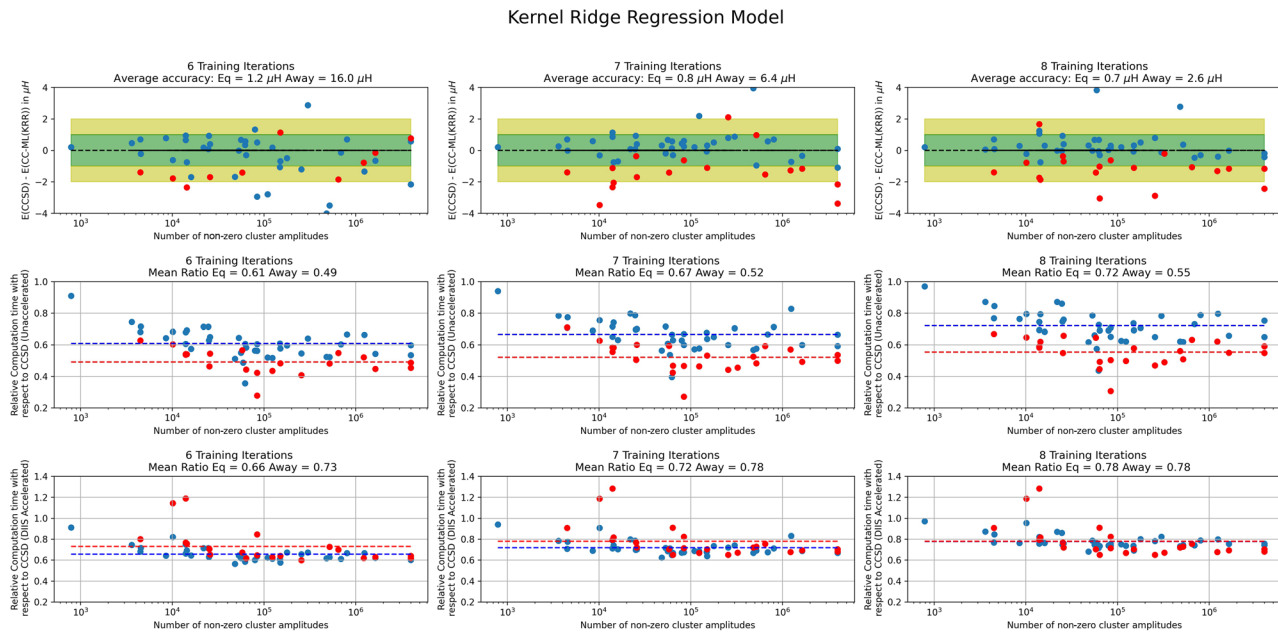


FIG. 2. Performance of the hybrid CC-ML(KRR) model: the x axes on all sub-plots are arranged in the increasing number of the non-zero cluster amplitudes, which is taken as a measure of the system size. The blue dots in all sub-plots are for the molecules in their respective equilibrium geometries, and the red dots are for the molecules in stretched geometries. The first row shows the difference in energy between the CC-ML(KRR) and exact CCSD. The black horizontal line is the reference, and the green horizontal bar signifies the convergence accuracy of $\pm 1 \mu\text{H}$. The second row shows the relative time taken by CC-ML(KRR) with respect to the exact CCSD (without DIIS acceleration). The red and blue dashed lines show the mean fraction of the computational timing. The third row shows the time taken by CC-ML(KRR) with respect to the DIIS accelerated CCSD scheme. “Eq” and “Away” in the sub-figure captions refer to the molecules in their equilibrium and away from equilibrium geometries, respectively. The three columns denote the number of training iterations employed.

accurately predicted by the model. This makes the KRR model quite data intensive and takes a high number of initial iterations to train the data for sufficiently accurate results. Moving toward a map that is more consistent with the numerical pattern of the CC iteration scheme is expected to reduce the number of training iterations and the required dimension of the independent amplitude space. We have generated a new kernelization technique that is more consistent with the CC iteration scheme. As regularization often slows down the learning process, one may remove the ridge regularization from Eq. (8). In order to speed up the calculations and get as much features as possible from very less amount of input parameters, we go back to Eq. (7) and define our own custom made kernel function. Note that KRR uses a ready-made polynomial kernel available in the standard library; however, CKR is based on our own kernel matrix, which we integrated with the library of Scikit.

Following a similar philosophy as KRR, we define the input training matrix T^L and T^S exactly the same way as defined in Eqs. (2) and (4). To extract the input features from the T^L and T^S matrices, we define two different feature matrices:

- The Squared Root Euclidean Distance Matrix (EDM), or what has simply been defined as the distance matrix D in our earlier works.^{24,25} The elements of the distance matrix D is defined as

$$d_{ij} = \|\vec{x}_i - \vec{x}_j\|, \quad (9)$$

where \vec{x}_i is defined as the i th row of T^L .

- Linear Kernel (Q , elements denoted as q_{ij}) is defined as

$$Q = T^L (T^L)^T. \quad (10)$$

Both of the matrices are symmetric and of the size $m \times m$, where m is, as usual, the number of the training datasets. The EDM and the linear kernel matrix are the input to the kernel, and they work as feature extractors from the training data.

With these feature matrices, a new kernel is constructed with the combination of exponential and sinusoidal parts. The kernel K with elements k_{ij} , $i, j = \{1, 2, \dots, p\}$ can be written as

$$k_{ij} = \exp(-\sin(g_{ij} + l_{ij})), \quad (11)$$

where

$$g_{ij} = \exp(-\gamma * d_{ij}), \quad l_{ij} = \log(q_{ij}), \quad (12)$$

where γ is a hyper-parameter, which can be optimized.

Once the model is trained through the initial cycles, we first calculate the new kernel matrix, K_L , with the new input values of the principal amplitudes through the new vector T_{new}^L . In order to do so, we first calculate the feature extraction matrices, where the new

squared root EDM D_L is defined as

$$D_{L,i} = \sqrt{\sum_{k=1}^n (t_{(new)ik}^L - t_{ik}^L)^2}, \quad i = \{1, 2, \dots, m\} \quad (13)$$

and the linear kernel matrix Q_L as

$$Q_L = T^L (T_{new}^L)^T. \quad (14)$$

In Eqs. (9) and (10), we now replace the elements of D and Q matrices by the elements of the new feature matrices D_L and Q_L from Eqs. (13) and (14). Finally, using Eq. (11), we get the predicted auxiliary amplitudes as

$$t_{pred}^S = (K_L)^T K^{-1} T^S. \quad (15)$$

Although the hybrid CC–ML(CKR) model performs quite well in most of the cases, it is observed that due to the sinusoidal nature of the kernel matrix, sometimes for some highly fluctuating larger amplitudes, combined with a bad choice of γ , may make $(g_{ij} + l_{ij})$ inside the exponential lose its monotonic nature. In that case, K may contain a very small diagonal value, and taking its inverse via Eq. (15) makes the whole model to explode with a very large value of the predicted auxiliary amplitudes. Forceful regularization procedure on the diagonal values does not work well as it changes the overall nature of the kernel matrix, which later gives poor accuracy. One of the possible ways is to remove more fluctuating larger amplitudes from the training matrix itself before training. However, the removal of the highly fluctuating large amplitudes results in poorer accuracy of the overall model. Furthermore, extracting the highly oscillating large amplitudes beforehand is a highly nontrivial exercise in ML. A more stable model in this regard will be a subject of our forthcoming publication. In our model, to prevent this from happening, we integrated a separate algorithm which keeps track of the K_L matrix and prevents it from changing any of its element value by more than “0.02” by pushing it backward. This whole process makes the learning process slow and does not give the desired accuracy. Nonetheless, this procedure prevents the whole code from catastrophic breakdown. With this caveat, the results for the CKR model are discussed in the following.

2. Assessment of the performance of CKR model

It is evident from the previous discussion that the CKR method is a high-risk/high-profit model where for almost all the cases under consideration, one gets highly accurate results with less computation time compared to KRR. Like all other models considered in this paper, the accuracy largely depends on the number of training iterations. However, unlike KRR, the customized kernelization predicts the trajectory with less number of training iterations, and discarding the couple of initial iterations is not needed. This saves a significant computation time due to less training iterations. Moreover, the CKR model requires a much smaller size of the independent variables compared to KRR ($n_{L_{KRR}} \gg n_{L_{CKR}}$). This means that the major computational bottleneck of $n_L n_o^2 n_v^2$ scaling in step-II is significantly reduced. This thus allows a faster loop over the LAS elements, reducing the overall computation time significantly over KRR. Note that with a higher value of n_L , although the computation time increases slightly due to the $n_L n_o^2 n_v^2$ scaling in step-II, the results become significantly more accurate.

The performance of the hybrid CC–ML(CKR) model is shown in Fig. 3 for various numbers of the training iterations for about 43 different molecules/basis sets/geometries (see the [supplementary material](#) for details). With $m = 6$, the model is significantly less accurate than KRR with a MAD of 24.4 and 51.7 μH for molecules in equilibrium and away from equilibrium geometries, respectively, from the canonical CCSD calculations. However, the model has a sharper convergence with respect to the number of the training cycles compared to KRR. With $m = 8$, the MAD observed with the CKR model is only 2.9 μH for the molecules in equilibrium geometry, while for the molecules with away from equilibrium geometry, the MAD is about 4.2 μH . As we mentioned before, unlike KRR, one does not need to discard the initial iterations to train the model, and hence, the training can be performed with less number of iterations effectively. This amounts to significant reduction in the computation time than KRR. This is reflected in the second and third row panels of Fig. 3 where we have plotted the relative time requirement compared to the conventional CCSD. Note that for $m = 8$, the average time requirement to obtain energy of μH precision is only 55% of that of the canonical CCSD calculation for molecules in equilibrium. To achieve a similar accuracy for the molecules with distorted geometry, the average time requirement is about 45% compared to canonical CCSD. If the canonical CCSD calculations are accelerated by DIIS as is done in most of the cases, the time requirement for the hybrid CC–ML(CKR) slightly goes up to 60% on an average to the DIIS accelerated CCSD calculation. However, one should monitor the predicted energy from CKR as in few rare cases, the model may get unstable as mentioned before, producing somewhat inaccurate energy.

C. Polynomial kernel ridge regression model

1. Working principles

The polynomial kernel ridge regression model has a similar structure to that of the CKR model presented in Sec. III B, and hence again, we only present the essential aspects which distinguish PKR from KRR. While the KRR model is linear by default, there is supposed to have more variational flexibility by introducing the nonlinear terms in the kernel function. To proceed along this direction, we define the input T^L and T^S matrices the same way as Eqs. (2) and (4). Furthermore, we define the linear kernel, Q , as Eq. (10). We then introduce our polynomial kernel K as

$$K = (\gamma Q + C)^o, \quad (16)$$

where $C = 1$ is a constant and $o = 3$ is the order of the polynomial. These values of C and o are taken by default in the ML library.²⁷ Like the previous two models, this kernel is now used in training of the amplitudes. The prediction is done by a similar technique used in the KRR model using Eq. (8). The most fundamental difference between the KRR and PKR is in the choice of the kernel function: while the former uses a linear regression type fitting, the latter uses polynomial function in this case of degree 3 for a better accuracy.

2. Assessment of the performance of PKR model

The PKR method is a variant of the parent KRR model. This model, as mentioned previously, increases the dimension of the feature matrix, which allows us a better fit of the auxiliary amplitudes in terms of the principal amplitudes. The PKR model, as a

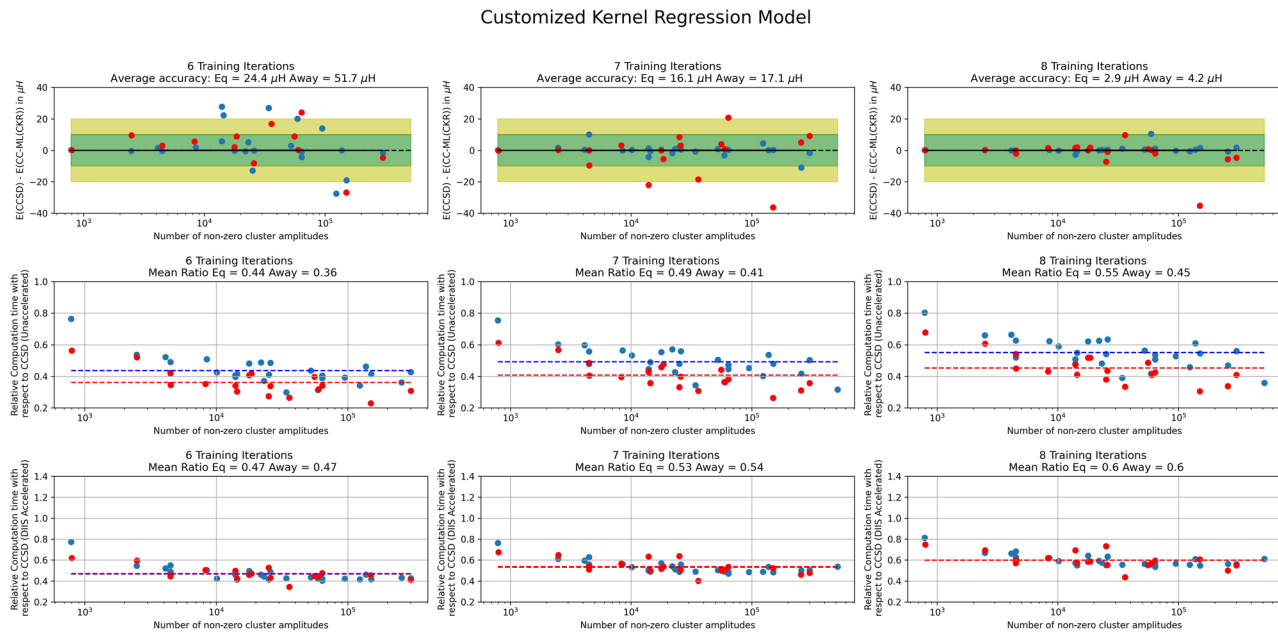


FIG. 3. Performance of CC-ML(CKR). The first row shows the difference in energy between the CC-ML(CKR) and the exact CCSD with the green bar showing an energy accuracy of $\pm 10 \mu\text{H}$. The second and third rows show the relative computational time of CC-ML(CKR) with respect to CCSD (without DIIS acceleration) and DIIS accelerated CCSD schemes, respectively. The three columns denote the number of training iterations employed for training. All other details are same as Fig. 2.

result, is highly accurate. However, like CKR, this too does not discard any initial iterations and hence has a similar requirement of the number of training cycles as that of CKR. Since the number of independent degrees of freedom increases due to the polynomial structure of the kernel via Eq. (5), a small dimension of the LAS, n_L , is sufficient to achieve high accuracy. The performance of the hybrid CC-ML(PKR) model is shown in Fig. 4 as a function of different numbers of the training iterations for about 61 different molecules/basis sets/geometries. For further information on the molecules, geometries, and basis sets employed in this study, see the [supplementary material](#). With $m = 6$, the model is less accurate than KRR with a MAD of 16.1 and $37.6 \mu\text{H}$ for molecules in equilibrium and away from equilibrium geometries, respectively, from the canonical CCSD calculations. This is substantially better than CKR model with equal number of training iterations. Even though the model has a sharper convergence of the estimated energy than KRR, it is not as sharp as CKR. This is presumably due to the fact that the PKR model, by construction, starts with an unknown polynomial mapping, and it also has a ridge regularization term. With $m = 8$, the MAD for the PKR model goes down to $3.4 \mu\text{H}$ for the molecules in equilibrium geometry and $7.1 \mu\text{H}$ for those in the away from equilibrium geometry. PKR, due to its inherent polynomial structure, does not require to discard any initial iterations to construct the kernel, and hence, there is a significant reduction in the computation time than KRR. Moreover, PKR requires a very small dimension of the principal amplitude space, n_L , like CKR. This leads to the time requirement of PKR very similar to CKR. Following discussions from previous models, we note that for $m = 8$, the average time requirement is only 55% of that of the canonical CCSD calculation

for molecules in equilibrium. To achieve a similar accuracy for the molecules with distorted geometry, the average time requirement is about 44% compared to canonical CCSD. If the canonical CCSD calculations are accelerated by DIIS, the time requirement for the hybrid CC-ML(PKR) slightly goes up to 60% on an average to the DIIS accelerated CCSD calculation with $m = 8$. The model is, however, much more stable than CKR due to inclusion of regularization terms via Eq. (8).

D. K-nearest neighbors regression model

1. Working principles

The K-nearest neighbor model, although primarily is a classification model, can be cast into one of the simplest regression model in machine learning, involving much less complex kernels as compared to the usual kernels which were discussed previously for other sophisticated regression based models. This thus allows us to examine the circular causality framework with minimum numerical coupling support and almost works as the benchmark of the worst accuracy bound for working with regression models. In the following, we briefly discuss how KNN can be modified slightly to turn it into an approximate regression model.

Traditionally, the KNN is used to classify a quantity into groups looking at nearest points through features such as Euclidean or Manhattan distance. Here, we have used the Euclidean distance as the measure of the closeness. The neighbors are defined as the individual training iterations. Therefore, with m training iterations, we get m neighbors, each neighbor having an input principal amplitude feature matrix defined as $T_j^L = \{t_{ij}^L, i \in (1, n_L)\}$ and output as

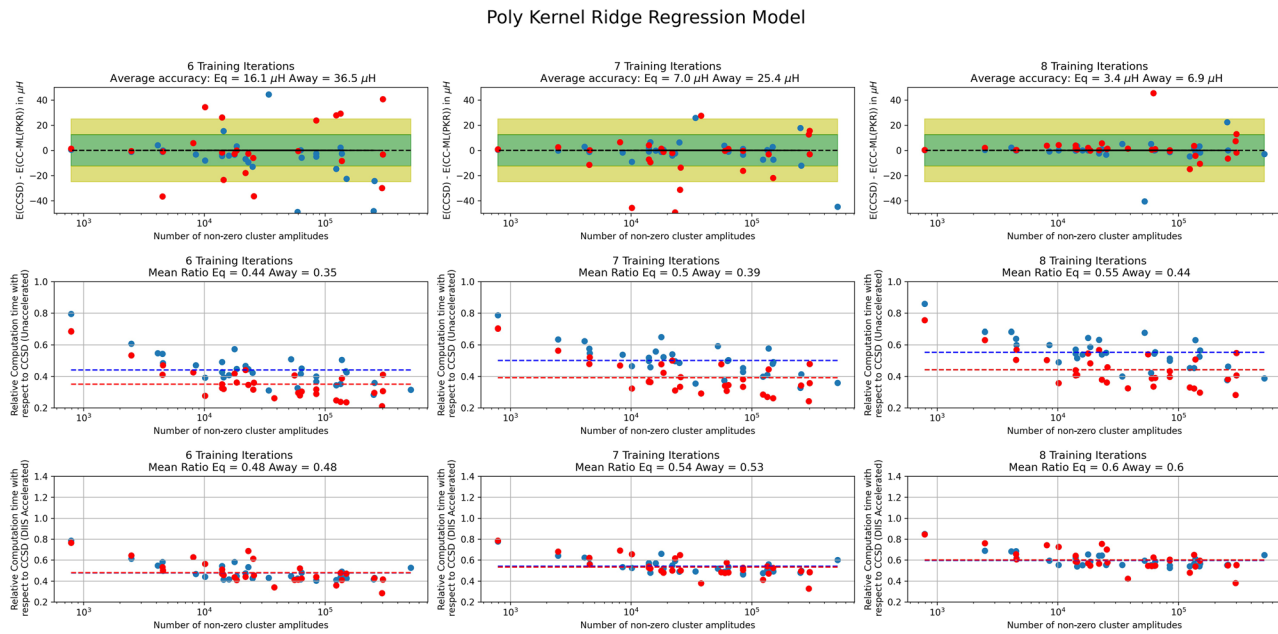


FIG. 4. Performance of CC-ML(PKR). The first row shows the difference in energy between the CC-ML(PKR) and the exact CCSD with the green bar showing an energy accuracy of $\pm 12.5 \mu\text{H}$. The second and third rows show the relative computational time of the model with respect to unaccelerated and DIIS accelerated CCSD schemes, respectively. The three columns are for three different training iterations ($m = 6, 7, 8$). All other details are same as Fig. 2.

the remaining auxiliary amplitudes $T_j^S = \{t_{ij}^S, i \in (1, n_S)\}$, where j is the number of the training iterations. At the end of the training iterations, we have m feature vectors and m output vectors. After starting the reduced iteration, we calculate the t_{new}^L using CC via step-II of the circular causality loop, and the t_{new}^S is predicted as an average of the k nearest neighbors, and its equation is given as

$$t_{new}^S = \frac{1}{k} \sum_i^k T_i^S, \quad (17)$$

where the nearness is defined as the Euclidean distance between t_{new}^L and t^L from earlier iterations. As is clear, the “nearness” of a point is completely arbitrary, and we noticed that at just one neighbor, the accuracy nearly saturated and did not increase with the increase in the number of neighbors. It is not always necessary that the accuracy would increase with the increase in neighbors as it may lead to overfitting. With these ideas in mind and through a well established ML library,²⁷ we converted our ML model to be of KNN-regression form. In the subsequent paragraph, we demonstrate the performance of the model over several test cases.

2. Assessment of the performance of KNN model

In Fig. 5, we have presented the performance of KNN for 51 molecular systems in their equilibrium and away from equilibrium geometries. Clearly, the model does not perform nearly well as compared to the other robust regression models discussed previously. While the average deviation improves sharply by taking high number of training iterations, with fewer training iterations, the model performs poorly. This contradicts the basic idea of supervised

machine learning where we target to model the CC iteration convergence with only a few number of training cycles. This is primarily due to it being a classification model, rather than a regression based model. While the process of training remaining the same, which guarantees that it takes approximately similar computational time to CKR and PKR, the accuracy is not nearly as good as that of the previously discussed models. We must also note that being a rudimentary model, it provides us with a base case, and any sophisticated machine learning model would be an improvement over it. Thus, the use of such a classification based model is not recommended to simulate the CC iteration series.

IV. STATISTICAL ERROR DISTRIBUTION: DISCUSSION AND SUMMARY

Through this work, we have thoroughly benchmarked some of the common supervised machine learning models based on the regression technique to solve CC equations. The average accuracy and computation time requirements for various models under consideration are summarized in Table I. The CC-ML(KRR) seems to be the most stable and robust model with guaranteed convergence beyond μH at the cost of large number of training iterations. The model saves around 30%–40% computation time over the unaccelerated canonical CCSD calculations and 20%–30% computation time over the DIIS accelerated CCSD calculations. The bottleneck for the CC-ML(KRR) model is the high number of iterations required for the training on top of a few discarded initial iterations. The CC-ML(CKR) and CC-ML(PKR) perform much better in terms

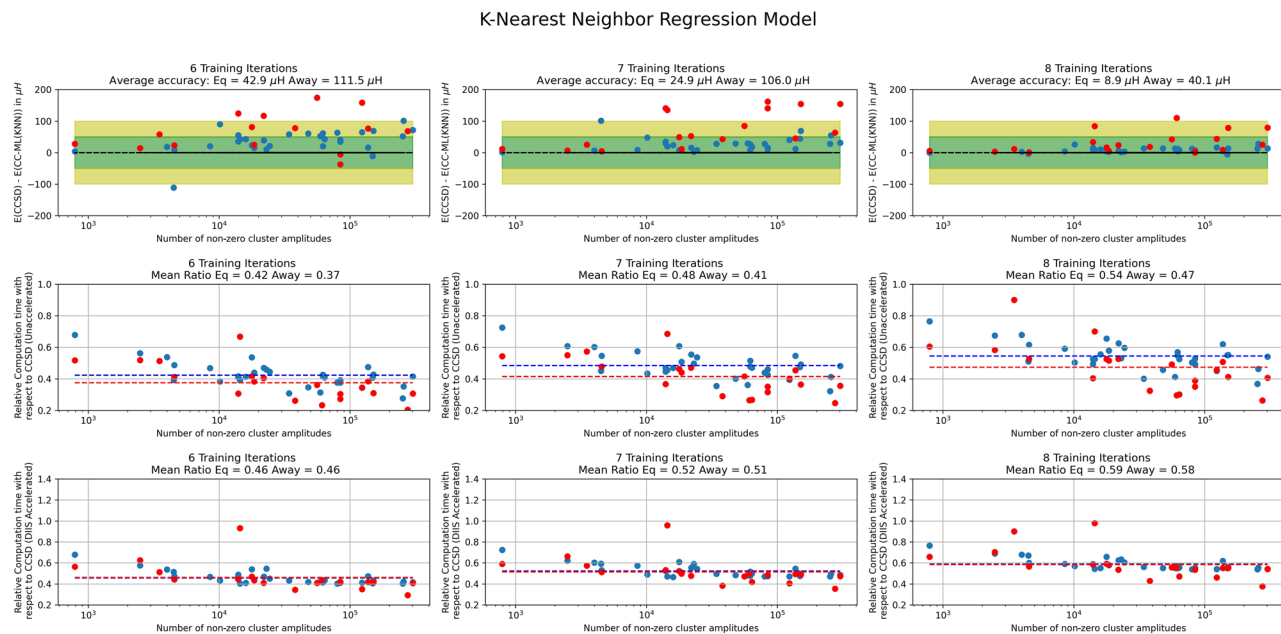


FIG. 5. Performance of CC-ML(KNN): the first row shows the difference in energy between the CC-ML(KNN) and exact CCSD with the green bar showing an energy accuracy of $\pm 50 \mu\text{H}$. The second and third rows show the relative computational time of the model with respect to unaccelerated and DIIS accelerated CCSD schemes, respectively. The three columns are for three different training iterations ($m = 6, 7, 8$). All other details are same as Fig. 2.

of the time requirement since it can be trained with a fewer number of iterations without discarding the initial steps. For both the models, the accuracy is marginally poorer than the CC-ML(KRR) model, although the average error in both the cases is only a few μH irrespective of the molecular correlation complexity. Apart from that, a relatively “loose” classification based KNN machine learning model gives a respectable accuracy of $9 \mu\text{H}$ for molecules

in equilibrium geometries and $40 \mu\text{H}$ in geometries away from the equilibrium with the time saving similar to the previous two models.

Furthermore, in Fig. 6, we have done a more rigorous statistical analysis of the error for each of these models. In separate subplots, we have shown the distribution of error through the histogram for various models and various number of training iterations. In all the

TABLE I. Performance of the different machine learning models. The accuracy is defined as the absolute difference of the energy obtained by the hybrid CCSD-ML model and the canonical CCSD. The time/CCSD(UA) denotes the fraction of time taken by the CC-ML model with respect to the unaccelerated CCSD scheme. The time/CCSD(DIIS) denotes the fraction of time taken by the CC-ML model with respect to a DIIS based CCSD method. All the models, particularly those based on regression, provide excellent accuracy with substantial savings in computational time.

| Parameters | n_{train} | Machine learning models | | | | | | | |
|----------------------------|--------------------|-------------------------|------|------|------|------|------|------|-------|
| | | KRR | | CKR | | PKR | | KNN | |
| | | Eq. | Away | Eq. | Away | Eq. | Away | Eq. | Away |
| Accuracy (μH) | 6 | 1.2 | 16.0 | 24.4 | 51.7 | 16.1 | 37.6 | 42.9 | 111.5 |
| | 7 | 0.8 | 6.4 | 16.1 | 17.1 | 7.0 | 26.2 | 24.9 | 106.0 |
| | 8 | 0.7 | 2.6 | 2.9 | 4.2 | 3.4 | 7.1 | 8.9 | 40.1 |
| Time/CCSD(UA) | 6 | 0.61 | 0.49 | 0.44 | 0.36 | 0.44 | 0.35 | 0.42 | 0.37 |
| | 7 | 0.67 | 0.52 | 0.49 | 0.41 | 0.5 | 0.39 | 0.48 | 0.41 |
| | 8 | 0.72 | 0.55 | 0.55 | 0.45 | 0.55 | 0.44 | 0.54 | 0.47 |
| Time/CCSD(DIIS) | 6 | 0.66 | 0.73 | 0.47 | 0.47 | 0.48 | 0.48 | 0.46 | 0.46 |
| | 7 | 0.72 | 0.78 | 0.53 | 0.54 | 0.54 | 0.53 | 0.52 | 0.51 |
| | 8 | 0.78 | 0.78 | 0.59 | 0.6 | 0.6 | 0.6 | 0.59 | 0.58 |

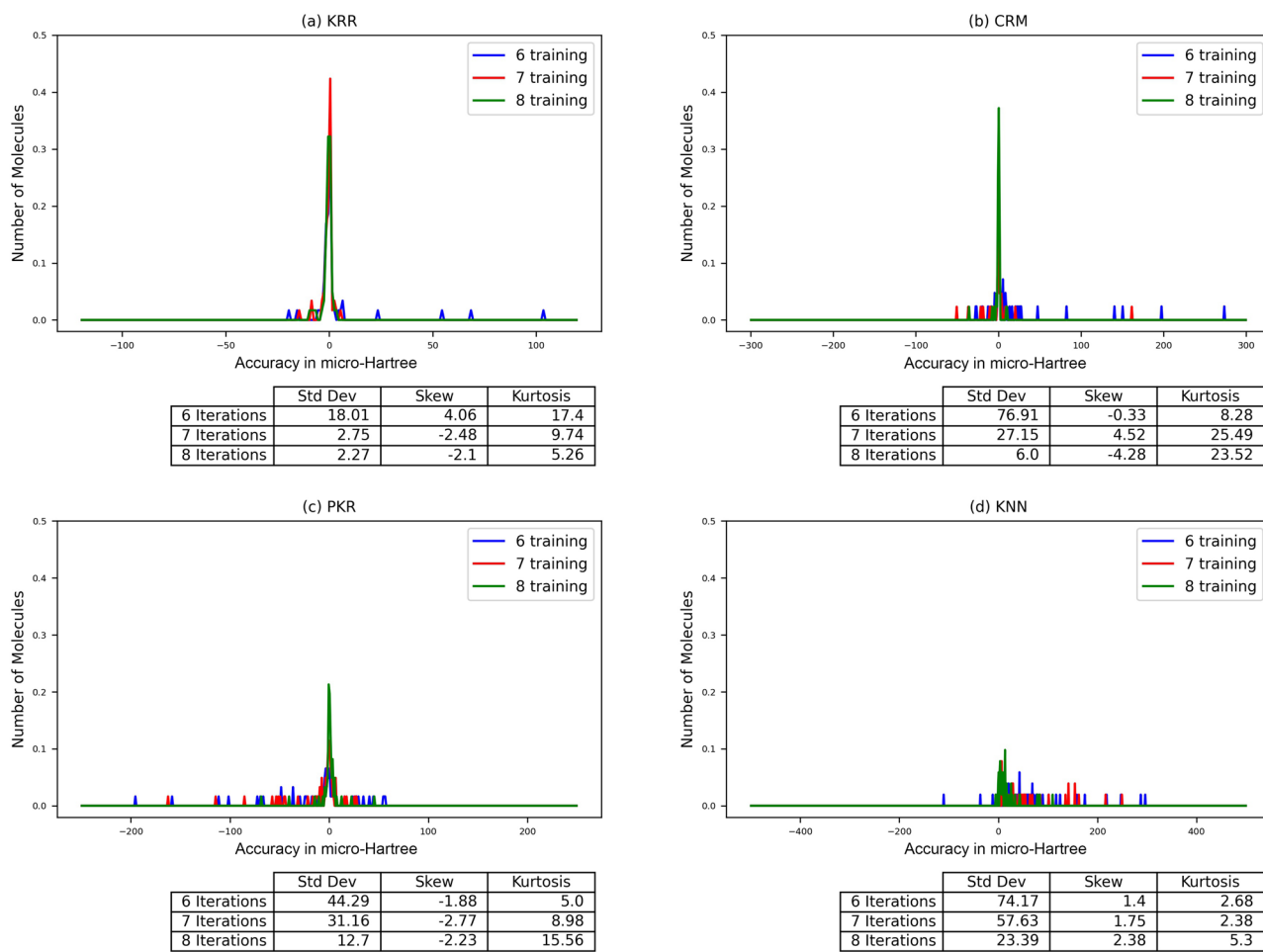


FIG. 6. Statistical analysis of error for each model. In all the models, the standard deviation decreases as one increases the number of training iterations. The leptokurtic nature of the distribution is due to a few outliers, although the accuracy systematically improves in all molecules for all the models, as evident from the standard deviation.

models under consideration, the standard deviation (SD) becomes successively smaller with the number of training iterations, indicating that most of the data get clustered around the mean value. Except PKR, the convergence with respect to the number of training cycles for most of the molecules is not monotonic. This leads the error distribution to be alternatively negative and positively skewed as one increases m . Although the increase in the number of training iterations progressively improves the SD for a few exceptional systems, particularly for CKR and PKR, the accuracy does not improve significantly. This renders into leptokurtic (kurtosis greater than 3) nature of the error distribution with high peakedness around the mean and a few elements in a heavier tail. For a couple of molecules that form these extreme outliers contributing to the heavy tail, we have analyzed their convergence with respect to the number of training iterations, and they are presented in the [supplementary material](#) along with the convergence of the same molecules with other models (see the [supplementary material](#), Fig. S1). KRR, being the most stable model, seems to perform best, which

systematically improves the accuracy for all the molecular systems under consideration.

It should be noted that for molecules in highly stretched geometries or for strongly multireference systems, even eight training iterations may not be sufficient for accuracy $\sim \mu E_h$. This is primarily due to the fact that the initial iterations for such cases that are used for training are too random to build a good model, and hence, they at times do not converge to a good agreement. However, in such complicated systems, the canonical CCSD calculations take unusually high number of iterations to converge. Therefore, with a similar time fraction typical for each model, one would be able to accommodate more than eight or nine training iterations for a good accuracy. We have shown a couple of such prototypical cases (stretched ethene with twice equilibrium bond lengths and C dimer) in the [supplementary material](#) (Figs. S2 and S3, respectively).

We conclude that overall, the hybrid CC-ML technique is statistically stable and could be used as a standardized method of calculation. The method works well with several supervised machine

learning models and is highly tunable as per the requirement of accuracy and cost affordability. Irrespective of the model used, one way to improve the accuracy is to provide higher variational flexibility in F by choosing a lower value of the threshold ϵ (that is increasing n_L for LAS). This is also a demonstration of the robustness of the synergistic interdependence of the cluster amplitudes and the resulting hybrid CC-ML models under various electronic complexities. In our implementation, the construction of the diagrams for only the selected excitations belonging to the LAS, as shown in step-II (Fig. 1), is far from being optimal, and there is plenty of room to further improve upon. This would further reduce the computation time significantly. We note that the hybrid CC-ML scheme does not require any previously computed data; rather, they can be trained on the fly based on the various cluster amplitudes determined at the initial steps during the optimization process for individual molecules.

V. FUTURE DIRECTIONS

This work reinforces the synergistic interrelation of the cluster amplitudes during the CC iteration scheme and demonstrates the effectiveness of the hybrid CC-ML methodology. However, being one of the first instances of the numerical inclusion of synergetics via ML in CC, the possibilities are endless. Since the field of ML is still new, development of better models that resonate with the exact analytical structure of the CC iteration scheme would be an exciting avenue to explore. The development of an analytical mapping is a highly non-trivial challenge. While the adiabatic decoupling scheme to map the auxiliary amplitudes in terms of the principal amplitudes is available²⁸ in the literature, conversion of the technique to machine learning based methods for numerical efficiency is a challenge. Other areas of work would be the inclusion of DIIS in the CC-ML technique for even faster calculations. Since the LAS dimension grows only sub-linearly with inclusion of higher order excitations (such as triples and quadruples), we expect to have further computational gain for the CCSDT/CCSDTQ level of theories. Thus, the development and implementation of hybrid CCSDT/CCSDTQ-ML scheme would be an interesting avenue to venture. In addition, this would enable high order calculations with large basis sets faster in the near future. An extension of this model to treat molecular excited states would also be a subject to a forthcoming publication.

SUPPLEMENTARY MATERIAL

The [supplementary material](#) contains the geometry and basis sets of the molecules employed for each model in the study. In addition, the convergence of the results for each model as a function of the number of training iterations for a few prototypical cases, including highly stretched ethene and C_2 , is presented.

ACKNOWLEDGMENTS

The authors thank Mr. Anish Chakraborty for many stimulating discussions about the structure of the program. R.M. thanks IRCC, Indian Institute of Technology, Bombay, for the research

seed grant, and SERB, Department of Science and Technology, Government of India, for their financial support.

AUTHOR DECLARATIONS

Conflict of Interest

The authors have no conflicts to disclose.

Author Contributions

S.R. and K.K.S. contributed equally to this work.

DATA AVAILABILITY

The data that support the findings of this study are available from the corresponding author upon reasonable request.

REFERENCES

- ¹J. Čížek, "On the correlation problem in atomic and molecular systems. Calculation of wavefunction components in Ursell-type expansion using quantum-field theoretical methods," *J. Chem. Phys.* **45**, 4256–4266 (1966).
- ²J. Čížek, "On the use of the cluster expansion and the technique of diagrams in calculations of correlation effects in atoms and molecules," *Adv. Chem. Phys.* **14**, 35–89 (1969).
- ³J. Čížek and J. Paldus, "Correlation problems in atomic and molecular systems III. Rederivation of the coupled-pair many-electron theory using the traditional quantum chemical methods," *Int. J. Quantum Chem.* **5**, 359–379 (1971).
- ⁴R. J. Bartlett and M. Musial, "Coupled-cluster theory in quantum chemistry," *Rev. Mod. Phys.* **79**, 291 (2007).
- ⁵P. Pulay, "Convergence acceleration of iterative sequences. The case of scf iteration," *Chem. Phys. Lett.* **73**, 393–398 (1980).
- ⁶P. Pieuch and L. Adamowicz, "Solving the single-reference coupled-cluster equations involving highly excited clusters in quasidegenerate situations," *J. Chem. Phys.* **100**, 5857–5869 (1994).
- ⁷E. F. Kjønstad, S. D. Folkestad, and H. Koch, "Accelerated multimodel Newton-type algorithms for faster convergence of ground and excited state coupled cluster equations," *J. Chem. Phys.* **153**, 014104 (2020).
- ⁸C. Yang, J. Brabec, L. Veis, D. B. Williams-Young, and K. Kowalski, "Solving coupled cluster equations by the Newton Krylov method," *Front. Chem.* **8**, 590184 (2020).
- ⁹R. M. Parrish, Y. Zhao, E. G. Hohenstein, and T. J. Martínez, "Rank reduced coupled cluster theory. I. Ground state energies and wavefunctions," *J. Chem. Phys.* **150**, 164118 (2019).
- ¹⁰R. Schutski, J. Zhao, T. M. Henderson, and G. E. Scuseria, "Tensor-structured coupled cluster theory," *J. Chem. Phys.* **147**, 184113 (2017).
- ¹¹A. E. DePrince III and C. D. Sherrill, "Accuracy and efficiency of coupled-cluster theory using density fitting/Cholesky decomposition, frozen natural orbitals, and at 1-transformed Hamiltonian," *J. Chem. Theory Comput.* **9**, 2687–2696 (2013).
- ¹²M. Schütz and F. R. Manby, "Linear scaling local coupled cluster theory with density fitting. Part I: 4-external integrals," *Phys. Chem. Chem. Phys.* **5**, 3349–3358 (2003).
- ¹³H. Haken and A. Wunderlin, "Slaving principle for stochastic differential equations with additive and multiplicative noise and for discrete noisy maps," *Z. Phys. B: Condens. Matter* **47**, 179–187 (1982).
- ¹⁴H. Haken, "Nonlinear equations. The slaving principle," in *Advanced Synergetics: Instability Hierarchies of Self-Organizing Systems and Devices* (Springer, Berlin, Heidelberg, 1983), pp. 187–221.
- ¹⁵H. Haken, "Synergetics: An overview," *Rep. Prog. Phys.* **52**, 515–553 (1989).
- ¹⁶N. Marwan, M. Carmenromano, M. Thiel, and J. Kurths, "Recurrence plots for the analysis of complex systems," *Phys. Rep.* **438**, 237–329 (2007).
- ¹⁷N. Marwan, M. C. Romano, M. Thiel, and J. Kurths, Recurrence plots; accessed May 19, 2020.
- ¹⁸K. P. Murphy, *Machine Learning: A Probabilistic Perspective* (MIT Press, 2012).

- ¹⁹M. Urban, J. Noga, S. J. Cole, and R. J. Bartlett, "Towards a full CCSDT model for electron correlation," *J. Chem. Phys.* **83**, 4041–4046 (1985).
- ²⁰Y. S. Lee and R. J. Bartlett, "A study of Be₂ with many-body perturbation theory and a coupled-cluster method including triple excitations," *J. Chem. Phys.* **80**, 4371–4377 (1984).
- ²¹P. Piecuch, J. A. Hansen, and A. O. Ajala, "Benchmarking the completely renormalised equation-of-motion coupled-cluster approaches for vertical excitation energies," *Mol. Phys.* **113**, 3085–3127 (2015).
- ²²J. Shen and P. Piecuch, "Merging active-space and renormalized coupled-cluster methods via the CC ($P; Q$) formalism, with benchmark calculations for singlet-triplet gaps in biradical systems," *J. Chem. Theory Comput.* **8**, 4968–4988 (2012).
- ²³G. Beylkin, L. Monzón, and X. Yang, "Adaptive algorithm for electronic structure calculations using reduction of Gaussian mixtures," *Proc. R. Soc. A* **475**, 20180901 (2019).
- ²⁴V. Agarwal, A. Chakraborty, and R. Maitra, "Stability analysis of a double similarity transformed coupled cluster theory," *J. Chem. Phys.* **153**, 084113 (2020).
- ²⁵V. Agarwal, S. Roy, A. Chakraborty, and R. Maitra, "Accelerating coupled cluster calculations with nonlinear dynamics and supervised machine learning," *J. Chem. Phys.* **154**, 044110 (2021).
- ²⁶H. Q. Minh, P. Niyogi, and Y. Yao, "Mercer's theorem, feature maps, and smoothing," in *International Conference on Computational Learning Theory* (Springer, 2006), pp. 154–168.
- ²⁷F. Pedregosa, G. Varoquaux, A. Gramfort, V. Michel, B. Thirion, O. Grisel, M. Blondel, P. Prettenhofer, R. Weiss, V. Dubourg, J. Vanderplas, A. Passos, D. Cournapeau, M. Brucher, M. Perrot, and E. Duchesnay, "Scikit-learn: Machine learning in Python," *J. Mach. Learn. Res.* **12**, 2825–2830 (2011).
- ²⁸V. Agarwal, C. Patra, and R. Maitra, "An approximate coupled cluster theory via nonlinear dynamics and synergetics: The adiabatic decoupling conditions," *J. Chem. Phys.* **155**, 124115 (2021).